Demographic stochasticity and resource autocorrelation control biological invasions in heterogeneous landscapes

Andrea Giometto, Florian Altermatt and Andrea Rinaldo

A. Giometto (http://orcid.org/0000-0002-0544-6023) (andrea.giometto@gmail.com) and A. Rinaldo, Laboratory of Ecohydrology, School of Architecture, Civil and Environmental Engineering, École Polytechnique Fédérale de Lausanne, CH-1015 Lausanne, Switzerland. AG also at: Dept of Molecular and Cellular Biology, Harvard Univ., Cambridge, MA, USA. AR also at: Dipto di Ingegneria Civile, Edile ed Ambientale, Univ. di Padova, Padua, Italy. – AG and F. Altermatt (http://orcid.org/0000-0002-4831-6958), Eawag, Swiss Federal Inst. of Aquatic Science and Technology, Dept of Aquatic Ecology, Dübendorf, Switzerland. FA also at: Dept of Evolutionary Biology and Environmental Studies, Univ. of Zürich, Zürich, Switzerland.

Mounting theoretical evidence suggests that demographic stochasticity, environmental heterogeneity and biased movement of organisms individually affect the dynamics of biological invasions and range expansions. Studies of species spread in heterogeneous landscapes have traditionally characterized invasion velocities as functions of the mean resource density throughout the landscape, thus neglecting higher-order moments of the spatial resource distribution. Here, we show theoretically that different spatial arrangements of resources lead to different spread velocities even if the mean resource density throughout the landscape is kept constant. Specifically, we find that increasing the resource autocorrelation length causes a reduction in the speed of species spread. The model shows that demographic stochasticity plays a key role in the slowdown, which is strengthened when individuals can actively move towards resources. We then experimentally corroborated the theoretically predicted reduction in propagation speed in microcosm experiments with the protist *Euglena gracilis* by comparing spread in landscapes with different resource autocorrelation lengths. Our work identifies the resource autocorrelation length as a key modulator and a simple measure of landscape susceptibility to biological invasions, which needs to be considered for predicting invasion dynamics within naturally heterogeneous environmental corridors.

Environmental fluctuations and heterogeneity are ubiquitous in nature and are thought to affect nearly all aspects of ecology, ranging from species coexistence to population synchrony, driving range shifts and potentially causing abrupt biotic change (With and Crist 1995, With 2002). Local population dynamics in temporally fluctuating environments have been studied extensively in recent years (Gonzalez and Holt 2002, Duncan et al. 2013), mainly with respect to population synchrony (Benton et al. 2001, Fox et al. 2011). Theoretical (Vasseur 2007), experimental (Gonzalez and Holt 2002, Fontaine and Gonzalez 2005, Massie et al. 2015) and field (García-Carreras and Reuman 2011) studies have highlighted the relevance of the temporal autocorrelation structure of environmental fluctuations for ecological processes. In fact, environmental variables are typically positively correlated (Benincà et al. 2011), that is, events that are closer in time or in space are more likely to be similar. Focusing on environmental autocorrelation is also of interest in view of the global shift towards 'bluer' climate variables (i.e. more fluctuating) across most continents (García-Carreras and Reuman 2011). Whereas the ecological significance of temporal fluctuations of the environment has received much investigation, the implications of environmental heterogeneity on spatial dynamics received surprisingly little attention (With 2002, Melbourne et al. 2007). The effect of spatial heterogeneity of process rates or resource distributions may be especially relevant in the context of biological invasions and range shifts (Hastings et al. 2005, Börger et al. 2008).

Natural environments are almost universally heterogeneous (Holyoak et al. 2005). Much of the current understanding of species spread, however, is based on theoretical models that consider homogeneous landscapes (i.e. landscapes where vital rates and mobility are uniform in space). Traditionally, the propagation of invasive fronts has been modeled with the Fisher–Kolmogorov equation (Fisher 1937, Kolmogorov et al. 1937). This non-linear reaction–diffusion equation was applied extensively to describe field data (Lubina and Levin 1988, Andow et al. 1990). Stochastic generalizations of the Fisher–Kolmogorov equation showed that demographic stochasticity affects the propagation dynamics in uniform landscapes, causing a reduction in the front propagation speed (Hallatschek and Korolev 2009) and an intrinsic variability of the process across replicated invasions (Giometto et al. 2014). In recent years, progress has been achieved in the theoretical understanding of species spread in more

complex, heterogeneous or fluctuating environments (Neubert et al. 2000, Melbourne et al. 2007, Dewhirst and Lutscher 2009, Méndez et al. 2010, Pachepsky and Levine 2011, Fronhofer et al. 2017). For example, the study of front propagation in landscapes whose spatial structure includes a complex topology suggests that the presence of bifurcations along the backbone of the propagation may reduce the invasion speed (Méndez et al. 2003, 2004, Campos et al. 2006, Bertuzzo et al. 2007). Temporal fluctuations in mean dispersal distances were shown to increase the front propagation velocity (Ellner and Schreiber 2012), while temporally uncorrelated fluctuations in demographic parameters were shown to typically reduce it (Méndez et al. 2011).

Here, we focus on biological invasions in landscapes characterized by temporally invariant but spatially heterogeneous resource distributions, which could, for example, reflect the spatial composition and quality of soil, gap dynamics in forests and subsequent light availability for understory plants and their associated herbivore fauna or habitat fragmentation due to human land-use (With and Crist 1995, With 2002). The investigation of species spread in spatially heterogeneous landscapes has mainly focused on the relationship between the mean invasion speed and the percentage of favorable habitat across the landscape (With and Crist 1995, With 2002, Dewhirst and Lutscher 2009), showing that spread may not occur below minimal thresholds of suitable growth habitat. A limited number of empirical works has measured spread rates in heterogeneous and diverse habitats and compared realized spread distances in patchily distributed sites (Bergelson et al. 1994, Bailey et al. 2000, Williams et al. 2016a, b) or across landscapes with monotonic gradients (Fronhofer et al. 2017). Spatially heterogeneous landscapes, however, are not only characterized by the mean percentage of favorable habitat or the mean density of resources, but crucially also by their spatial autocorrelation. Currently, we lack both theoretical and experimental studies investigating the role of such autocorrelation in driving the spread of species.

In our experiment we manipulated the availability of light as a limiting resource with a spatially heterogeneous distribution. Light is the most important resource for photosynthetically active organims, such as higher plants or algae, and these organisms are not only using light as their key resource for growth, but can also adjust their movement in response of light availability (Giometto et al. 2015). Such directional movement can be active movement (e.g. in flagellated algae) or indirected growth/budding of plant stolones. For most plants, especially in forests, the availability of light is spatially highly heterogeneous, and mostly driven by gap dynamics (Kricher 2011). Thus, gaps due to tree-fall or anthropogenic activities create a patchy distribution of light as a key resource for understory plants, and all of their associated interacting herbivores and pollinators. We were interested in how the arrangement, specifically the autocorrelation of the light availability, can affect spread dynamics of organisms. While we focus on light as a resource, our theoretical work and paralleled experiments are more generic with respect to the specific resource creating the heterogeneity in habitat quality.

Here, we theoretically and experimentally show that the invasion speed is affected not only by the mean amount of resources along the landscape (or, analogously, by the percentage of suitable habitat), but also by their spatial autocorrelation structure. We find that environmental heterogeneity and demographic stochasticity jointly affect biological invasions. In particular, we show that it is necessary to include demographic stochasticity in models of spread in order to properly understand biological invasions in spatially heterogeneous environments. Our investigation is organized as follows. We first show theoretically, in two models of invasion at different levels of biological detail, that the speed of species spread decreases when the resource autocorrelation length increases. Second, we verify such a prediction in a microcosm experiment with the flagellated protist *Euglena gracilis*, by manipulating light intensity profiles along linear landscapes (light is an energy source for *E. gracilis*, as it has chloroplasts and can photosynthesize). Third, we discuss the contribution of each process included in the model to the propagation of biological invasions.

Methods

Model

Species spread in heterogeneous linear landscapes is modeled via a stochastic generalization of the Fisher–Kolmogorov equation including demographic stochasticity (Dornic et al. 2005, Bonachela et al. 2012, Giometto et al. 2014, Villa Martín et al. 2015):

$$\frac{\partial \rho}{\partial t} = D \frac{\partial^2 \rho}{\partial x^2} + r(I)\rho \left[1 - \frac{\rho}{K}\right] + \sigma \sqrt{\rho} \eta \qquad (1)$$

where $\rho(x,t)$ is the density of individuals, D is the diffusion coefficient of the species due to the active movement of individuals, r is the growth rate, K is the carrying capacity, σ is a parameter describing the amplitude of demographic stochasticity and η is a gaussian, zero-mean white noise (i.e. the noise has correlations $\langle \eta(x,t)\eta(x',t')\rangle = \delta(x - x')\delta(t - t')$, where δ is the Dirac's delta function). Itô's stochastic calculus is adopted, as appropriate for the demographic noise term (Giometto et al. 2014). The diffusion term in Eq. 1 assumes random movement of individuals. The growth rate $r_i = r_0 I$ is assumed to be a function of the local amount of resources $I(x)$, which can assume two values: $I(x) = 1$ or $I(x) = 0$. Landscape heterogeneity is thus embedded in the resource profile $I(x)$. We studied the dimensionless form of Eq. 1, which reads (Supplementary material Appendix 1):

$$\frac{\partial \rho'}{\partial t'} = \frac{\partial^2 \rho'}{\partial x'^2} + \chi_I \rho'[1 - \rho'] + \sigma'' \sqrt{\rho'} \eta \qquad (2)$$

where $t' = r_0 t, x' = \sqrt{D/r_0} x, \rho' = \rho/K, \sigma'' = \dfrac{\sigma}{(K^2 r D)^{1/4}}$ and $\chi_I(x')$ is the indicator function of the set of x' for which $I(x') = 1$. In the following we drop primes for convenience: one can recover the original dimensions by multiplying t by r_0, x by $\sqrt{r_0/D}$ and rescaling ρ and σ as indicated above. Numerical integration of stochastic partial differential equations with square root noise terms require ad hoc numerical methods, as standard approaches such as the first-order explicit Euler method inevitably produce unphysical negative values for the density ρ (Dornic et al. 2005). Therefore, Eq. 2 was integrated with the split-step method proposed in Dornic et al. (2005) (see Supplementary material Appendix 1 for details).

We generated landscapes with various resource autocorrelation lengths by imposing $I(x)$ to be composed of subsequent independent patches of suitable ($I(x) = 1$ and $r = r_0$) or unsuitable ($I(x) = 0$ and $r = 0$) habitats (Fig. 1A). The length of each patch was drawn from an exponential distribution with rate μ. Therefore, each landscape was a stochastic realization of the so-called telegraph process with rate μ and autocorrelation length $c_L = 1/(2\mu)$ (Supplementary material Appendix 1). The mean extent of suitable and unsuitable patches in such landscapes is $1/\mu$. Because simulated landscapes were finite, we only accepted landscapes with mean resources equal to $\bar{I} = 1/L \int_0^L I(x)\,dx = 1/2$ and autocorrelation length confined to a narrow window around $1/(2\mu)$. Examples of landscapes used in the simulations are shown in Fig. 1A.

We generated 96 landscapes for each value of resource autocorrelation length c_L and integrated Eq. 2 numerically for each landscape and for each value of $\sigma \in \{0.1, 0.2, 0.4, 0.6\}$ (Fig. 1B), with initial density profiles localized at the origin. A reflective boundary condition at the origin may cause the extinction of the whole population, which may happen
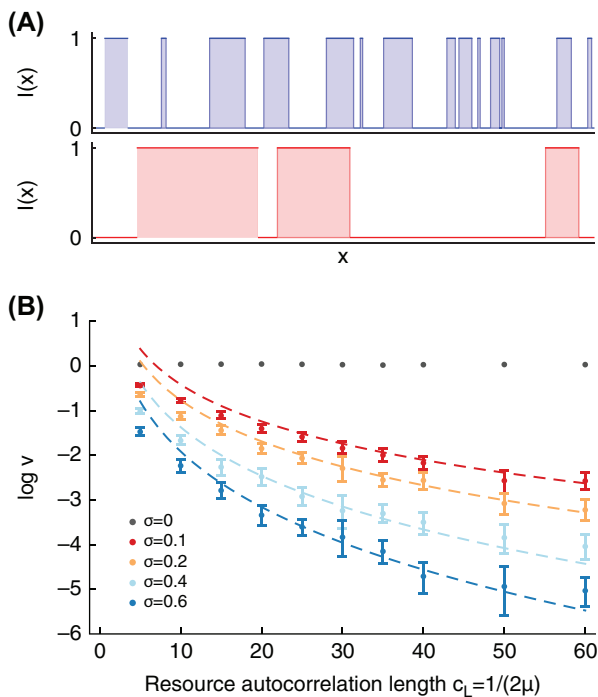

(A)

(B)

Figure 1. Mean front propagation in the model (dimensionless Eq. 2). (A) Examples of landscapes with different resource autocorrelation length c_L, generated via the telegraph process with rate μ. (B) The mean invasion speed computed in numerical integrations of the model (Eq. 2) decreases with increasing resource autocorrelation length c_L (log-linear plot) for $\sigma > 0$ and is a decreasing function of the amplitude of demographic stochasticity σ (different colors according to legend). With $\sigma = 0$ the dynamics is deterministic and the mean front propagation speed does not decrease with c_L (gray dots). Error bars display the 95% confidence interval for $\log(v)$, computed with 2×10^3 bootstrap samples. Error bars for $\sigma = 0$ are smaller than symbols. Dashed lines show the mean front propagation speed computed according to the theoretical approximation (Eq. 4).

due to demographic stochasticity. Because our investigation is only concerned with successful invasions (i.e. invasions that survive an initial establishment phase), we fixed the left boundary at $\rho = 1$, which thus represents a continuous source of individuals. Such a boundary condition ensures that the population does not go extinct in our numerical investigation. For each numerical integration, we measured the position of the front by fixing a threshold value of the density ($\bar{\varrho} = 0.15$) and recording the furthest point from the origin where the cell density was higher than such value. The mean propagation speed for each value of the resource autocorrelation length was computed by fitting a straight line (least-squares fit) to the mean front position versus time in the asymptotic propagation regime (Supplementary material Appendix 1 Fig. A6), before any of the replicated invasions reached the end of the landscape.

The traditional way to compute the invasion speed in the deterministic Fisher–Kolmogorov equation is to analyze the traveling wave solutions of the equation. Such procedure cannot be adopted for Eq. 2, due to the stochastic noise term. We derived a theoretical approximation to the mean front propagation speed, valid for large autocorrelation length c_L and σ (Supplementary material Appendix 1 section 2.1.2), by characterizing the mean time taken to cross a patch of unfavorable habitat (where $I = r = 0$) of length z. Such mean time is shown (Supplementary material Appendix 1) to depend on z and σ as $\langle \tau \rangle (z, \sigma) = Cz^2 e^{d(z\sigma^b)^a}$, where C, a, b and d are constants, independent of z and σ. Additionally, we characterized the functional dependence of the variance of τ on z and σ and derived an approximation to the variance of the total time taken by a front to colonize completely a landscape of finite length L (Supplementary material Appendix 1). Our approximation is in good agreement with numerical integrations of Eq. 2 (Fig. 1).

To test whether deterministic models predict a slowdown of the invading front for increasing resource autocorrelation length, we numerically integrated Eq. 2 with $\sigma = 0$. Additionally, we numerically integrated Eq. 2 with $\sigma = 0$ imposing a negative growth rate r in unfavorable patches where $I = 0$ (Supplementary material Appendix 1).

Experiments

We performed experiments with the flagellated protist *Euglena gracilis*, acquired from Carolina Biological Supply (NC, USA). A culture of *E. gracilis* was initialized two weeks prior to the start of the experiment and kept at 22°C under constant LED light of wavelength 469 nm (emission width approximately 10 nm), in a filtered (0.2 μm filter) nutrient medium composed of sterilized spring water and protozoan pellets at a density of 0.45 g l⁻¹ in a 500 ml Schott flask (for details on the experimental system see Altermatt et al. 2015). Such a model system has been used successfully in previous experiments to investigate ecological and evolutionary dynamics during range expansions (Giometto et al. 2014, 2015, Fronhofer and Altermatt 2015, Seymour et al. 2015, Gounand et al. 2017).

In our experiment, light was used as the energy source for *E. gracilis*. To demonstrate that light was crucial for the growth of *E. gracilis* in our experimental setting, we measured *E. gracilis'* growth curves (Fig. 4A) by initializing eight

low-density cultures in 10 ml cell culture flasks. Half of such cultures were placed on top of two LEDs (for each culture) operated at a total flux of 1 mW each. The other half of the cultures were placed on top of two LEDs (for each culture) operated at the same power, but covered with black tape so that no light would penetrate. The spatial arrangement of illuminated and non-illuminated cell culture flasks was randomized.

Light also affects the movement behavior of *E. gracilis* individuals through a process known as phototaxis, the directed movement of cells towards or away from light (Drescher et al. 2010, Giometto et al. 2015). Specifically, at low to intermediate light intensities, *E. gracilis* swims towards the light source at a time scale much shorter than the typical generation time. At very high light intensities, negative phototaxis can also be observed, and the plastic reaction of phototaxis can be induced very reliably (Giometto et al. 2015). The light intensity value used in our experiments is smaller than the light intensity value at which negative phototaxis occurs.

The front propagation experiment was performed in linear landscapes, which were channels drilled on a plexiglass sheet (5 mm wide, 3 mm deep and 1.9 m long, respectively, 300, 200 and 10^5 times the size of an individual, Giometto et al. 2013), filled with filtered nutrient medium (Fig. 2A). A gasket avoided water spillage and a plexiglass lid was used to seal the system. The experimental replicates were kept in a climatized dark room at 22°C for the whole duration of the experiment. Each linear landscape was covered by a black cardboard sheet. Heterogeneous distributions of resources were generated via linear arrays of LEDs (Fig. 2B) controlled via Arduino Uno boards. LEDs in the array were separated by a distance of $\Delta L = 3.12$ cm from each other and could be switched on or off individually. Switched-on LEDs emitted light with an intensity of 5.2 W m^{-2} within the plexiglass channel, immediately above the LED. The linear landscapes were placed on top of the LED array at a distance of 4.5 mm. The light intensity profile generated by one LED was measured by placing a white paper sheet inside the plexiglass channel and by measuring the irradiance on the sheet with a digital camera operated in grayscale. The total radiant flux of the LED was measured via a calibrated photodiode. Light intensity profiles with the desired autocorrelation length were designed by imposing the probability λ of the LED number i + 1 in the LED array to be switched-on if the LED number i was switched-off, that is, P[LED(i + 1) = ON|LED(i) = OFF] = λ. Such Markov Chain was imposed to be symmetric, that is, P[LED(i + 1) = OFF|LED(i) = ON] = λ. Small and large values of λ generate resource distributions with long and small autocorrelation lengths (approximately equal to ΔL/(2λ)), respectively. Because landscapes were of finite total length, the above procedure could generate by chance resource profiles with autocorrelation length different from the desired one and with a mean frequency of switched-on LEDs different from 1/2. Therefore, the set of resource profiles obtained with the above Markov Chain procedure was restricted to those with a mean frequency of switched-on LEDs equal to 1/2 and in a narrow window of autocorrelation length around the desired one. Therefore, all replicates had the same mean light intensity equal to $\bar{I} = 1/L \int_0^L I(x)\,dx$.

We compared two treatments in the experiment. Treatment 1 consisted of landscapes with identical small autocorrelation length ($c_L \simeq 2$ cm) but different switched-on LED sequences, generated via the Markov chain procedure with λ = 0.75. Treatment 2 consisted of landscapes with identical large autocorrelation length ($c_L \simeq 6$ cm) but different switched-on LED sequences, generated via the Markov chain procedure with λ = 0.25. The choice of the large autocorrelation length value in the experiment was limited by the total finite length of the experimental setup and was chosen to be less than 1/20 of the total setup length. We initially had six landscape replicates of each treatment, but lost one replicate of treatment 1 due to leakage. All 11 landscapes had the same total number of switched-on LEDs and the experimental light intensity
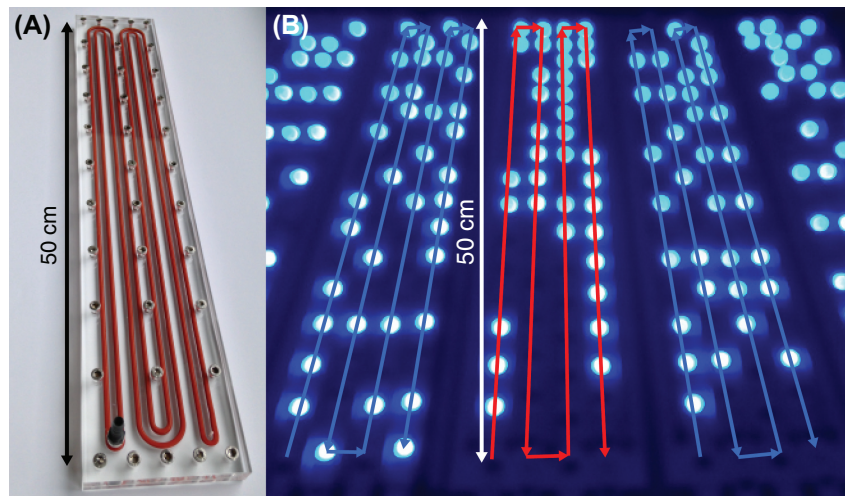

Figure 2. Experimental setup. (A) Linear landscapes used in the experiments were channels drilled on a plexiglass sheet. A gasket (orange rubber band) avoided water spillage. (B) Photograph of the LED strips used to control the distribution of resources for *E. gracilis*. The red and blue lines show the paths of landscapes with large and small resource autocorrelation length, respectively.
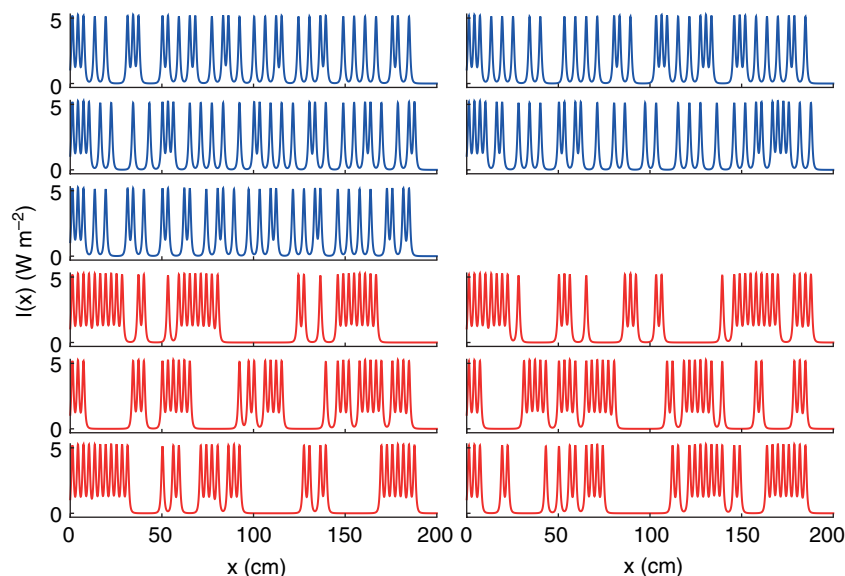
Figure 3. Light intensity profiles used in the experiment. One spread experiment was performed for each landscape. The total light intensity is the same for each landscape. Landscapes with the same color have identical small (blue) or large (red) autocorrelation length of the resource distribution I(x), but different LED on-off sequences.

profiles are shown in Fig. 3. The stated values of autocorrelation length are based on the first-order autocorrelation of the Markov chain that generated the landscape. The first three LEDs in every landscape were switched-on to allow the local establishment of the inoculated *E. gracilis* population and to avoid differences between the two treatments in the initial establishment dynamics. Thus, the landscapes generated via the Markov chain procedure described in the text started at the fourth LED. In treatment 2 (large autocorrelation length), three landscapes were chosen so that the fourth LED was switched on and the other four were chosen so that the fourth LED was switched off. In other words, the realized Markov chain started from its stationary distribution. The spatial arrangement of landscapes belonging to the two treatments on the experimental bench was randomized.

At the start of the experiment, we introduced an ensemble of *E. gracilis* individuals at one end of the linear landscapes. Following the inoculation, we measured for eight consecutive days the density of *E. gracilis* throughout all replicates by taking pictures with a stereomicroscope equipped with a digital camera and counting individuals via image analysis (Altermatt et al. 2015).

Statistical analysis

We used a mixed effect model to compare the speed of the propagating *E. gracilis* among the two different treatments. Thereby, the autocorrelation treatment was included as a fixed effect, while day and replicate were included as random effect. We repeated this analysis using different choices of threshold values used for determining the front position. The minimum and maximum threshold values employed in the statistical analysis were chosen such that no replicate displayed a retreating front between successive measurements (caused by noise in the density profiles). The test statistics are reported in Table 1 for the density threshold value

$\bar{\rho} = 60$ cm^{-1} and in the Supplementary material Appendix 1 Table A1 for all values of ρ considered. We did not include the first timepoint in the analysis because it was measured immediately after the inoculation of *E. gracilis* in the landscape and thus was identical for all replicates. Because the propagating front reached the end of the landscape at day 4 in some replicates, the front propagation analysis was performed only with the data up to day 3 (included) to avoid spurious border effects due to the finite size of the system.

Model with directed movement towards resources

Equation 1 does not assume directed movement of individuals towards resources. This directed movement, however, occurs in our experiment and is likely to occur in nature (Andow et al. 1990, Börger et al. 2008, Fronhofer et al. 2017). Additionally, the experimental resource distributions (i.e. the light intensity profiles I(x)) were not simply sequences of illuminated and non-illuminated spatial patches with sharp edges, but, rather, smooth light intensity profiles alternating between well-lit and dark regions of the landscape according to the spatial arrangement outlined above. Because *E. gracilis* is capable of detecting light intensity gradients and moving towards well-lit regions of the landscape, this directed movement may affect the invasion dynamics. To assess the net contribution of the directed

Table 1. Mixed-effect test statistics testing the speed of front propagation, with the autocorrelation length treatment as single fixed effect and time/replicate as random effect. The treatment with small autocorrelation length had five replicates, the treatment with large autocorrelation length had six replicates. The front position was measured at the density threshold value $\bar{\rho} = 60$ cm^{-1}.

	Value	SE	df	t-value	p-value
Intercept	45.98	3.27	44	14.04	p < 10^{-4}
Autocorrelation length	−11.61	4.43	9	−2.62	0.0279

movement of individuals towards resources, we incorporated in Eq. 1 the model for phototaxis derived in Giometto et al. (2015). The phototactic term was inferred from measurements of stationary density distributions of *E. gracilis* in the presence of light gradients (such measurements were performed with the same experimental system adopted here) and was shown to reproduce the accumulation dynamics of *E. gracilis* populations accurately in Giometto et al. (2015). The model equation reads:

$$\frac{\partial \rho}{\partial t} = \frac{\partial}{\partial x}\left[D\frac{\partial \rho}{\partial x} - \frac{\partial \varphi}{\partial x}(I)\rho\right] + r(I)\rho\left[1 - \frac{\rho}{K}\right] + \sigma\sqrt{\rho}\eta \qquad (3)$$

where $\varphi = \phi_0(I - I_C)/(I + I_r)$ is the phototactic potential describing *E. gracilis'* attraction towards (or against) light (Giometto et al. 2015). The parameters describing ϕ were estimated (Giometto et al. 2015) and were set equal to $\phi_0 = 1.4 \times 10^8$ m^4 W^{-1} s^{-1}, $I_r = 1.7$ W m^{-2} and $I_C = 28$ W m^{-2}. We assumed that r follows Monod kinetics (the assumption is customary for phytoplankton, Diehl 2002), that is, $r(I) = r_1 I/(I + K_I)$, where K_I is the half-saturation constant. The model (Eq. 3) was integrated with parameters suitable to describe the experimental system, $r_1 = 6\times10^{-3}$ min^{-1}, $K_I = 1$ W m^{-2}, $K = 300$ cm^{-1}, $D = 0.08$ cm^2 min^{-1} (estimated in Giometto et al. 2015), various values of σ (Supplementary materiual Appendix 1 Fig. A8) and initial condition localized at the origin. See Supplementary material Appendix 1 for details on the numerical integration scheme adopted. The slowdown effect caused by the resource autocorrelation structure is also found with other choices of the growth rate dependence on the resource density. In fact, we found that results do not change qualitatively by assuming a linear dependence of r on I. We used Eq. 3 to simulate biological invasions in linear landscapes with resource distributions I(x) exhibiting various autocorrelation lengths. To mimic the experimental setup (Fig. 3), numerical landscapes were generated with the same Markov-chain procedure used to design the experimental landscapes, where the light intensity profile generated by a single LED (centered in x = 0) was assumed equal to the best fit of the equation $I(x) = c_0 /(c_1^2 + x^2)^2$ to the measured light intensity profile (see Fig. S1 of Giometto et al. 2015). The total light intensity was kept constant for all landscapes. To further mimic the experiment, we set reflecting boundary conditions for the integration of Eq. 3 and simulations in which the population went extinct were excluded from the analysis. Therefore, the model Eq. 3 was specifically derived to reproduce as closely as possible the experimental system at hand. Landscapes used in the simulations were much longer (18 m) than those used in the experiment in order to avoid border effects. Such numerical settings allowed a clear identification of the invasion front and allowed simulating species spread in landscapes with very large autocorrelation length, which could not be investigated experimentally because of the finite size of the experimental setup.

Data deposition

Results

Our generalization of the Fisher–Kolmogorov equation (Eq. 1 and 2) includes demographic stochasticity and resource heterogeneity. Resource heterogeneity affects the spread dynamics through the dependence of the growth rate r on the local amount of resources I. We found that the speed of invasion in the model Eq. 2 decreases with increasing resource autocorrelation length (Fig. 1B). The mean front propagation speed, in heterogeneous landscapes where resource patch lengths are distributed exponentially with rate μ, depends on c_L and σ asymptotically (i.e. for large c_L and σ) as:

$$v = \frac{L}{\frac{\mu L}{2}\int_0^L dz \langle\tau\rangle(z,\sigma)\mu e^{-\mu z}} \simeq \frac{8c_L^2}{\int_0^\infty dz \langle\tau\rangle(z,\sigma)e^{-z/(2c_L)}} \qquad (4)$$

Figure 1B shows that Eq. 4 correctly predicts the speed of invasion at large values of c_L and σ. In heterogeneous landscapes with different spatial arrangements of favorable and unfavorable patches, if the percentage of space occupied by unfavorable patches is $f_0 \in (0,1)$ and the distribution of such patches lengths is $p_0(z)$, with mean $\int z\, p_0(z)dz = 1/\mu$, the asymptotic invasion velocity can be approximated as:

$$v = \frac{L}{\mu f_0 \int_0^\infty dz \langle\tau\rangle(z,\sigma)p(z)} \qquad (5)$$

We show in the Supplementary material Appendix 1 that Eq. 5 correctly predicts the speed of invasion in landscapes with percentages of unfavorable habitat different from $f_0 = 1/2$ (Supplementary material Appendix 1 Fig. A5). Note that the speed of invasion according to Eq. 4–5 is a function of the autocorrelation length if the landscapes consist of favorable and unfavorable patches generated through the telegraph process outlined in the Methods section. In general, however, the speed of invasion is not a one-to-one function of the resource autocorrelation length (or of other characteristic length scales of the landscape), but it rather depends on the whole distribution of unfavorable patch lengths through Eq. 5. The slowdown effect is due to the fact that, in the presence of demographic stochasticity, long patches of unfavorable habitat act as obstacles for the spread of populations. The larger the extent of the unfavorable patch, the longer it takes for a population to cross it. The front propagation speed is also found to be a monotonically decreasing function of the amplitude of demographic stochasticity (Fig. 1B). Accordingly, integrating the model without demographic stochasticity ($\sigma = 0$ in Eq. 2, gray dots in Fig. 1B) leads to no discernible slowdown of the front in strongly autocorrelated versus weakly autocorrelated landscapes, even when imposing negative values of the growth rate r in unfavorable patches where I = 0 (Supplementary material Appendix 1). Such results demonstrate that the local extinctions caused by demographic stochasticity in unfavorable patches are responsible for the observed front slowdown.

Numerical integration of Eq. 2 shows that the variability of the front position increases for larger values of c_L and σ. This increased variability is caused by two factors: 1) two landscapes with identical resource autocorrelation lengths appear increasingly dissimilar for increasing values of the
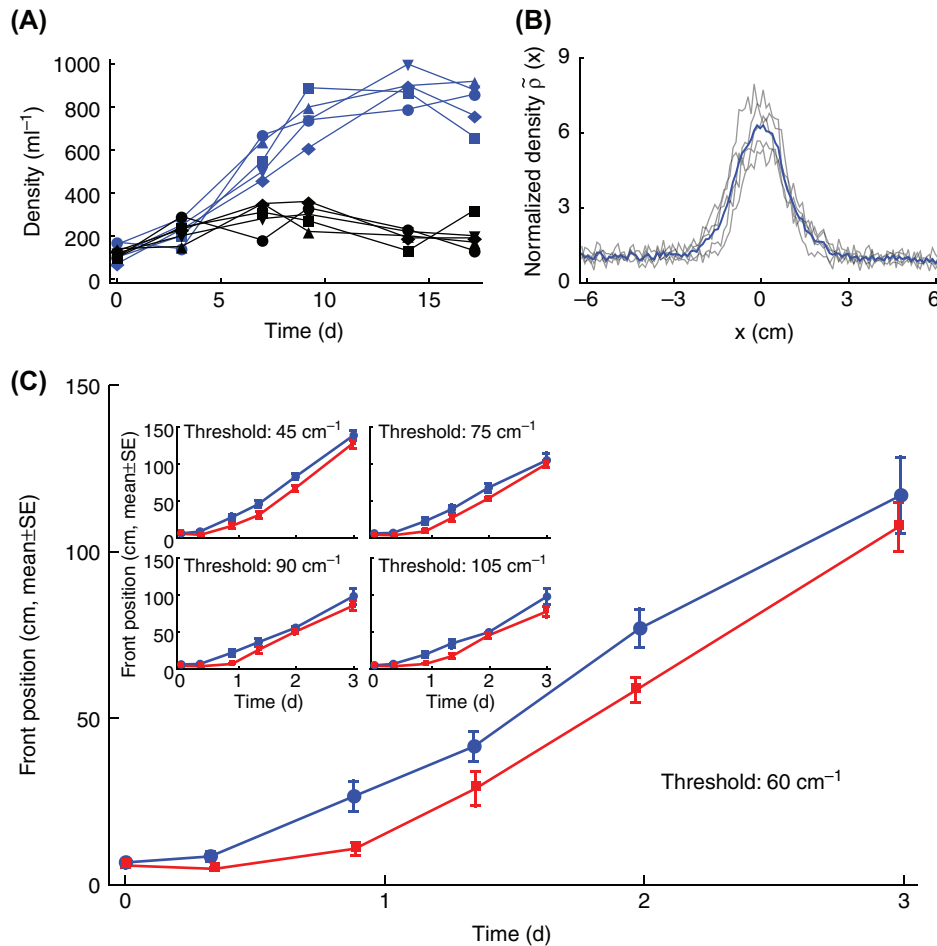
Figure 4. Experimental spread in autocorrelated landscapes. (A) Light was used as energy resource for *E. gracilis*. Replicated measured growth curves show that *E. gracilis* grows in the presence of light (blue symbols and lines) and does not grow in its absence (black symbols and lines). (B) Replicated measurements (gray lines) of *E. gracilis* density profiles (normalized by the value at the edge of the imaging window) in the presence of a LED at x = 0 cm show that *E. gracilis* populations accumulate around light sources through phototaxis. The blue line denotes the mean density profile across replicates (panel B is redrawn from Giometto et al. 2015). (C) Mean (± SE) position of the front, calculated among replicates with identical large (red) or small (blue) resource autocorrelation length at the threshold density value $\bar{\rho} = 60$ cm^{-1}. The inset shows mean front positions calculated at different threshold density values $\bar{\rho}$ as indicated. The slowdown effect is significant with all choices of $\bar{\rho}$ (Table 1).

typical patch length $1/\mu$; 2) the variance of the distribution of waiting times (i.e. the times to cross an unfavorable patch of length z) increases (approximately) quadratically with the mean time $\langle\tau\rangle(z,\sigma)$ (Fig. 3). These two observations can be used to approximate the fluctuations of the total time spent by the front colonizing a landscape of length L, as shown in the Supplementary material Appendix 1.

The model (Eq. 1, 2) assumes random local movement of individuals. Although such an assumption may be appropriate to describe spread in homogeneous landscapes (Andow et al. 1990, Giometto et al. 2014), individuals might be able to exploit local information on the availability of resources to direct their movement towards more favorable regions (Andow et al. 1990, Fronhofer et al. 2015). We studied the effect of biased movement towards resources by including an advection term (towards regions endowed with more resources) in Eq. 1, leading to Eq. 3. The latter model predicts again that the front propagation speed decreases for increasing resource autocorrelation length, in accordance with the former model (Eq. 1). Integrating Eq. 3 with and without

the advection term shows that the biased local movement towards resources causes an increased slowdown of the invasion front in strongly (compared to weakly) autocorrelated landscapes (Supplementary material Appendix 1 Fig. A8). In other words, the biased movement towards resources acts as a spring that keeps the population in favorable patches and works against the exploration of unfavorable ones. Excluding demographic stochasticity from the model Eq. 3 leads again to the elimination of the slowdown effect (inset of Supplementary material Appendix 1 Fig. A8).

In the subsequent experiment with *E. gracilis*, we observed a steady front propagation across all landscapes with a mean front propagation speed of 54 ± 9 cm day^{-1} (mean ± SD). The mean total number of individuals was 2420 ± 110 (mean ± SE) at the start of the experiment (day 0), $15\,000 \pm 800$ (mean ± SE) at the end of the front propagation phase (day 4) and $27\,000 \pm 4500$ (mean ± SE) at the end of the experiment (day 8). Thus, the invasion process was a combination of active, directed movement of individuals as well as reproduction. We found a significantly slower front propagation

in landscapes in which the resources were strongly spatially autocorrelated (mixed effect model p = 0.027, see also Table 1). The result is robust to changes of the threshold value at which the front position is evaluated (Table 1, Fig. 4C, Supplementary material Appendix 1 Fig. A9). The slowdown effect is visible in Fig. 4C, which shows the mean front position across replicated invasions in the two treatments.

Discussion

Our theoretical and experimental investigation highlights a yet unrecognized slowdown of biological invasions in heterogeneous landscapes with different resource autocorrelation lengths, which we then corroborated in experimental microcosms specifically designed to single out the effect of resource autocorrelation length on invasion speed. In the experiments, the demographic and movement traits of the study species were fixed and were inherent properties of the species. The accompanying models allowed to single out the individual role and the mutual interconnections of all processes included in the equations to the propagation dynamics in landscapes with different resource autocorrelation lengths.

Our model implicitly assumes that regions of the landscape with positive growth rate $r > 0$ can sustain a population of density K indefinitely. One could envision a more general scheme in which the spatial density of nutrients is fixed and finite at the start of the invasion and declines in time due to uptake by individuals. Investigation of such a model would allow us to test whether invasions in heterogeneous landscapes can proceed indefinitely and/or what is the probability that a population can overcome unfavorable patches of fixed length before becoming extinct due to the consumption of all the nutrients available in the colonized region of the landscape. In our experiments, we used light as the main energy source, which could be continuously provided at a fixed intensity. A natural analogue of this setting may be found in forest gap dynamics which are characterized by the low/high light availability in understory plant communities, or in aquatic systems differentially shaded by riparian vegetation. Note, however, that other nutrients in the medium provided the limiting resources which prevented the population from growing indefinitely. Because we did not observe the extinction of our experimental populations, we believe that a generalized model accounting for nutrient depletion behind the front goes beyond the scopes of this investigation, and would not affect our main conclusion.

Our theoretical and experimental study advances our current understanding of the spread of invading organisms in heterogeneous landscapes by addressing the joint effect of spatial environmental autocorrelation and demographic stochasticity on the spread dynamics. As arguably all natural landscapes are characterized by heterogeneous distributions of resources and all populations are subject to demographic stochasticity, our model incorporates two key elements (resource heterogeneity and demographic stochasticity) hitherto often overlooked in the modeling of biological spread.

A major result of our work is that demographic stochasticity is a key factor in the slowdown of front propagation in heterogeneous landscapes. Our finding highlights the importance of including demographic stochasticity in theoretical models because of the many facets through which it affects species spread (Hallatschek and Korolev 2009, Giometto et al. 2014) and ecological dynamics in heterogeneous landscapes (Villa Martín et al. 2015). The implications of the above results challenge the standard approach as stochastic effects are neglected by deterministic, Fisher–Kolmogorov-like models. Because the slowdown effect is only observed when demographic stochasticity is included in the models, our theoretical investigation suggests that the stochastic birth-and-death dynamics are the main drivers of the observed reduction in propagation speed, rather than the movement behavior of individuals in heterogeneous landscapes that has received so far most attention in the literature (Van Dyck and Baguette 2005, Börger et al. 2008). Previous studies have investigated the minimum percentage of suitable habitat that allows invasions to spread (With and Crist 1995, With 2002, Dewhirst and Lutscher 2009), suggesting that invasions cannot propagate in landscapes with mean resource density below a critical threshold. Our work shows, complementarily, that the spatial arrangement of resources affects species spread even if the total amount of available resources is kept constant. Thus, it is not only the mean resource density that matters for the front propagation dynamics, because the autocorrelation structure of landscape heterogeneity alone also affects species spread. In general, the larger the patch of unfavorable landscape, the longer it will take for the invading front to overcome it. Such a longer time is caused by the fact that a population cannot have net growth (on average) in an unfavorable patch, and is prone to local extinction due to demographic stochasticity. For large values of autocorrelation length, the mean speed of invasion is mainly determined by the time spent by the front trying to overcome long stretches of unfavorable landscape. In this limit, the mean speed of invasion is mainly determined by the distribution of unfavorable patches lengths, as captured by Eq. 4.

Our investigation also extends previous works that addressed the effect of temporal environmental fluctuations on species spread (Méndez et al. 2011, Ellner and Schreiber 2012) by showing that the autocorrelation length of the resource distribution should be added to the environmental factors that can slow species spread, along with temporal fluctuations of vital rates (Neubert et al. 2000, Ellner and Schreiber 2012), geometrical heterogeneities of the substrate (Méndez et al. 2003, 2004, Bertuzzo et al. 2007) and demographic stochasticity (Hallatschek and Korolev 2009). We note that our model does not account for Allee effects that may characterize the growth dynamics of a natural population, for example due to mate limitation. We anticipate that strong Allee effects (i.e. a negative growth rate at small population densities) might cause a reduction in the front propagation speed analogous to the one investigated here, caused by demographic stochasticity. In fact, the origin of such a slowdown effect lies in the local extinction of low-density populations that are able to diffuse through long stretches of unfavorable landscape. Such an extinction may be caused by either demographic stochasticity or by a strong Allee effect. Because our study species does not exhibit a noticeable Allee effect, we have not investigated its dynamics in this investigation.

The theoretical and experimental results reported here are in strong support and match to empirical real-world examples of invasions. For example, Bergelson et al. (1994) performed a field study with the invading weed *Senecio vulgaris* and found that the average spatial distance between two generations along linear transects increased when favorable patches were uniformly distributed in space (in the parlance of our work, the transect featured a small autocorrelation length), compared to transects with clumped patches (i.e. endowed with large autocorrelation length). Similar work exists by Bailey et al. (2000) on the spread of the fungal pathogen *Rhizctonia solani* and provides a complementing view to our investigation by evaluating the effect of the inter-distance between favorable patches on the spread and identifying experimentally the existence of a percolation threshold at a critical level of inter-patch distance. In the framework addressed here, the analog of such percolation threshold corresponds to an autocorrelation length much larger than the average distance traveled by the front during one generation. However, both of these studies also strongly differ from our work. Most importantly, biased active movement towards favorable patches was present in the experiment performed here and embedded in Eq. 3, while passive dispersal was implemented in Bergelson et al. (1994). Both Bailey et al. (2000) and Bergelson et al. (1994) differ from our study because the landscape and the distribution of resources herein are continuous, whereas they adopted discrete spatial distributions of favorable patches. Although such discrete distributions might provide a good approximation to some fragmented landscapes, continuous heterogeneous distributions may be equally likely to occur in nature.

Our results have important implications for species spread in natural environments, which are generally characterized by resources (seen as any field controlling vital rates, especially reproductive ones) being heterogeneously distributed. Specifically, we here provide a general theoretical framework to interpret the dynamical processes underlying the realized invasions. The typical autocorrelation length of the resource distribution can be inferred from environmental data (Urban et al. 2008) and can be used as a concise indicator for the propagation success of a species of interest. Furthermore, the spatial availability of resources is often altered by human activities, reinforcing the fragmentation of landscapes. In fact, habitat fragmentation may decrease significantly the autocorrelation length of the landscape through the introduction of qualitatively different patches in the natural environment (With and Crist 1995, With 2002, Holyoak et al. 2005). Our results give quantitative grounds to field observations on the effect of environmental heterogeneity on species spread. For instance, Lubina and Levin (1988) observed pauses in the spread of the California sea otter *Enhydra lutris* in the presence of habitat discontinuities. Such pauses and the corresponding piecewise-linear propagation of the front (see Fig. 2 of Lubina and Levin 1988) are also found in our model (Supplementary material Appendix 1 Fig. A7), which enables to relate the mean spatial extent of habitat discontinuities to the average speed of invasion through Eq. 4 and 5. An alternation between phases of halt and spread was also found in the range expansion of the cane toad *Chaunus marinus* in Australia (Fig. 2 of Urban et al. 2008). Urban et al. (2008) performed an in-depth analysis of the effect of environmental heterogeneity on the spread of the cane toad in the field and found a statistically significant effect of environmental heterogeneity and, most importantly, of the spatial autocorrelation of environmental variables on the realized patterns of invasion speed. They found such effect in nature in a realized (not replicable) invasion, and thus they could only correlate the realized spread dynamics and its reduction with the landscape autocorrelation. Here, we have given a mathematical framework and an experimental proof showing that the slowdown effect caused by the spatial autocorrelation structure of the landscape is not an artifact of the mathematical model.

Conclusion

In conclusion, our work demonstrates the need to account for the intrinsic stochasticity of population dynamics to broaden our understanding of ecological processes occurring in spatially extended natural landscapes, which typically display various degrees of heterogeneity. Further work should be dedicated to the modeling and experimentation of species spread in temporally varying landscapes and, possibly, spatially heterogeneous landscapes that fluctuate in time. Drawing from the literature on population dynamics in temporally fluctuating environments, understanding the causal link between the autocorrelation structure of fluctuations and the dynamics of species spread is a promising direction for future research in this area.

References

Altermatt, F. et al. 2015. Big answers from small worlds: a user's guide for protist microcosms as a model system in ecology and evolution. – Methods Ecol. Evol. 6: 218–231.

Andow, D. A. et al. 1990. Spread of invading organisms. – Landscape Ecol. 4: 177–188.

Bailey, D. J. et al. 2000. Saprotrophic invasion by the soil-borne fungal plant pathogen *Rhizoctonia solani* and percolation thresholds. – New Phytol. 146: 535–544.

Benincà, E. et al. 2011. Resonance of plankton communities with temperature fluctuations. – Am. Nat. 178: E85–E95.

Benton, T. G. et al. 2001. Population synchrony and environmental variation: an experimental demonstration. – Ecol. Lett. 4: 236–243.

Bergelson, J. et al. 1994. Rates of weed spread in spatially heterogeneous environments. – Ecology 74: 999–1011.

Bertuzzo, E. et al. 2007. River networks and ecological corridors: reactive transport on fractals, migration fronts, hydrochory. – Water Resour. Res. 43: W04419.

Bonachela, J. et al. 2012. Patchiness and demographic noise in three ecological examples. – J. Stat. Phys. 148: 723–739.

Börger, L. et al. 2008. Are there general mechanisms of animal home range behaviour? A review and prospects for future research. – Ecol. Lett. 11: 637–650.

Campos, D. et al. 2006. Transport on fractal river networks: application to migration fronts. – Theor. Popul. Biol. 69: 88–93.

Dewhirst, S. and Lutscher, F. 2009. Dispersal in heterogeneous habitats: thresholds, spatial scales and approximate rates of spread. – Ecology 90: 1338–1345.

Diehl, S. 2002. Phytoplankton, light and nutrients in a gradient of mixing depths: theory. – Ecology 83: 386–398.

Dornic, I. et al. 2005. Integration of Langevin equations with multiplicative noise and the viability of field theories for absorbing phase transitions. – Phys. Rev. Lett. 94: 100601.

Drescher, K. et al. 2010. Fidelity of adaptive phototaxis. – Proc. Natl Acad. Sci. USA 107: 11171–11176.

Duncan, A. B. et al. 2013. Stochastic environmental fluctuations drive epidemiology in experimental host–parasite metapopulations. – Proc. R. Soc. B 280: 20131747.

Ellner, S. P. and Schreiber, S. J. 2012. Temporally variable dispersal and demography can accelerate the spread of invading species. – Theor. Popul. Biol. 82: 283–298.

Fisher, R. A. 1937. The wave of advance of advantageous genes. – Ann. Hum. Genet. 7: 355–369.

Fontaine, C. and Gonzalez, A. 2005. Population synchrony induced by resource fluctuations and dispersal in an aquatic microcosm. – Ecology 86: 1463–1471.

Fox, J. W. et al. 2011. Phase locking, the Moran effect and distance decay of synchrony: experimental tests in a model system. – Ecol. Lett. 14: 163–168.

Fronhofer, E. A. and Altermatt, F. 2015. Eco-evolutionary feedbacks during experimental range expansions. – Nat. Commun. 6: 6844.

Fronhofer, E. A. et al. 2015. Condition-dependent movement and dispersal in experimental metacommunities. – Ecol. Lett. 18: 954–963.

Fronhofer, E. A. et al. 2017. Information use shapes the dynamics of range expansions into environmental gradients. – Global Ecol. Biogeogr. 26: 400–411.

García-Carreras, B. and Reuman, D. C. 2011. An empirical link between the spectral colour of climate and the spectral colour of field populations in the context of climate change. – J. Anim. Ecol. 80: 1042–1048.

Giometto, A. et al. 2013. Scaling body size fluctuations. – Proc. Natl Acad. Sci. USA 110: 4646–4650.

Giometto, A. et al. 2014. Emerging predictable features of replicated biological invasion fronts. – Proc. Natl Acad. Sci. USA 111: 297–301.

Giometto, A. et al. 2015. Generalized receptor law governs phototaxis in the phytoplankton *Euglena gracilis*. – Proc. Natl Acad. Sci. USA 112: 7045–7050.

Giometto, A. et al. 2017. Data from: Demographic stochasticity and resource autocorrelation control biological invasions in heterogeneous landscapes. – Dryad Digital Repository, <http://dx.doi.org/10.5061/dryad.51mq6>.

Gonzalez, A. and Holt, R. D. 2002. The inflationary effects of environmental fluctuations in source–sink systems. – Proc. Natl Acad. Sci. USA 99: 14872–14877.

Gounand, I. et al. 2017. Subsidies mediate interactions between communities across space. – Oikos 126: 972–979.

Hallatschek, O. and Korolev, K. 2009. Fisher waves in the strong noise limit. – Phys. Rev. Lett. 103: 108103.

Hastings, A. et al. 2005. The spatial spread of invasions: new developments in theory and evidence. – Ecol. Lett. 8: 91–101.

Holyoak, M. et al. 2005. Metacommunities: spatial dynamics and ecological communities. – Univ. of Chicago Press.

Kolmogorov, A. N. et al. 1937. A study of the diffusion equation with increase in the amount of substance, and its application to a biological problem. – Moscow Univ. Math. Mech. Bull. 1: 1–25.

Kricher, J. 2011. Tropical ecology. – Princeton Univ. Press, pp. 188–226.

Lubina, J. A. and Levin, S. A. 1988. The spread of a reinvading species: range expansion in the California sea otter. – Am. Nat. 131: 526–543.

Massie, T. M. et al. 2015. Enhanced Moran effect by spatial variation in environmental autocorrelation. – Nat. Commun. 6: 5993.

Melbourne, B. A. et al. 2007. Invasion in a heterogeneous world: resistance, coexistence or hostile takeover? – Ecol. Lett. 10: 77–94.

Méndez, V. et al. 2003. Speed of reaction-diffusion fronts in spatially heterogeneous media. – Phys. Rev. E 68: 041105.

Méndez, V. et al. 2004. Dynamical features of reaction–diffusion fronts in fractals. – Phys. Rev. E 69: 016613.

Méndez, V. et al. 2010. Reaction-transport systems. – Springer.

Méndez, V. et al. 2011. Effect of environmental fluctuations on invasion fronts. – J. Theor. Biol. 281: 31–38.

Neubert, M. G. et al. 2000. Invasion speeds in fluctuating environments. – Proc. R. Soc. B 267: 1603–1610.

Pachepsky, E. and Levine, J. M. 2011. Density dependence slows invader spread in fragmented landscapes. – Am. Nat. 177: 18–28.

Seymour, M. et al. 2015. Dendritic network structure and dispersal affect temporal dynamics of diversity and species persistence. – Oikos 124: 908–916.

Urban, M. C. et al. 2008. A toad more traveled: the heterogeneous invasion dynamics of cane toads in Australia. – Am. Nat. 171: E134–E148.

Van Dyck, H. and Baguette, M. 2005. Dispersal behavior in fragmented landscapes: routine or special movements. – Basic Appl. Ecol. 6: 535–545.

Vasseur, D. A. 2007. Environmental colour intensifies the Moran effect when population dynamics are spatially heterogeneous. – Oikos 116: 1726–1736.

Villa Martín, P. et al. 2015. Eluding catastrophic shifts. – Proc. Natl Acad. Sci. USA 112: E1828-E1836.

Williams, J. L. et al. 2016a. Rapid evolution accelerates plant population spread in fragmented experimental landscapes. – Science 353: 1–5.

Williams, J. L. et al. 2016b. The influence of evolution on population spread through patchy landscapes. – Am. Nat. 188: 15–26.

With, K. A. 2002. The landscape ecology of invasive spread. – Conserv. Biol. 16: 1192–1203.

With, K. A. and Crist, T. O. 1995. Critical thresholds in species' responses to landscape structure. – Ecology 76: 2446–2459.